A Broadband Dual-polarized Antenna with CRR-EBG Structure for 5G Applications

Peng Chen, Lihua Wang, and Tongyu Ding

Information Engineering College
Jimei University, Xiamen, Fujian, 361021, China
chenpeng@jmu.edu.cn, liliya@jmu.edu.cn, tyding@jmu.edu.cn

Abstract ─ In this paper, a broadband dual-polarized antenna with concentric rectangular ring electromagnetic bandgap (CRR-EBG) structure is proposed for 5G applications. The antenna consists of a pair of ±45° cross dipoles, an EBG array, and two inverted L-shaped improved feeding structures. In particular the ring part of the feeding structures can reduce the coupling between two ports. The leaky wave area of the EBG structure can be used to increase bandwidths. According to the measured results, the bandwidths of port1 and port2 are 32% (3.04-4.21GHz) and 28.3% (3.13-4.16GHz), respectively. The port-to-port isolation can reach up to 23 dB, and the average gain is approximately 5 dBi. The antenna has the advantages of a wide band, good isolation and a stable radiation pattern, which can be better used in 5G communications.

Index Terms ─ 5G, dual-polarized, electromagnetic band-gap (EBG), wideband.

I. INTRODUCTION

With the fast development of wireless communication systems and a looming shortage of wireless spectrum, the wireless industry has recognized the significance of multi-band and wideband antennas for future wireless communication systems [1-7]. In this sense, dual-polarized antennas, especially ±45° polarized antennas [8-11] have been widely proposed to determine multipath fading, pulling in signals from all directions better. It is worth noting that we added the electromagnetic band-gap (EBG) structure to the designed dual-polarized antenna for band spread.

The EBG structure is divided to a high-impedance surface (HIS) [12] and uniplanar compact (UC) surface [13-14]. In [15], the designed CSRR-EBG structures reduce the starting frequency of the first band gaps by 28%, and are used for multi-band applications. It is well known that for most dual-polarized antennas, such as those reported in [16] and [17], the stable unidirectional radiation pattern characteristics are mainly determined by the shape and size of the metal reflector. Since the antenna and reflector are generally one-quarter-wavelength apart, it is non-trivial to realize a low-profile antenna in this framework. On the contrary, owing to the in-phase reflection characteristic of EBG structure, the distance between antenna and reflector can be less than one-quarter-wavelength, and therefore reducing the size of the antenna [18]. EBG structure can also make use of leaky wave region to achieve bandwidth expansion [19-20] and better isolation [21-22]. In [23], Meander-Perforated Plane (MPP-EBG) structure was reported to improve the slow-wave effect, reduce the size and broaden the bandwidth.

In this paper, a broadband dual-polarized base-station antenna with CRR-EBG structure for 5G applications is proposed. The designed antenna provides good coverage of the frequency bands from 3.13 GHz to 4.16 GHz, intended for potential 5G applications. The simulated and measured results are obtained using Ansys HFSS 15, an Agilent vector analyzer and OTA. Detailed discussions of the design are provided as follows.

II. ANTENNA DESIGN

The geometric structure of the broadband dual-polarized antenna with EBG structure is presented in Figs. 1 and 2. The antenna is mainly composed of three parts: a pair of ±45° cross dipoles, an EBG array and two improved feeding structures with an inverted L-shaped structure. The three components are printed on an FR4 substrate with a relative dielectric constant of 4.4 and a thickness of 1 mm. The EBG structure attached to the lower dielectric plate consists of 48 units. If we remove the overlap the EBG structure and balun structure, the electromagnetic interference will be reduced.

The patch structure is composed of a pair of irregular hexagons dipole in Fig. 1 (b). Two pairs of small rectangles are formed on the dipoles, which are used to avoid short-circuit between the feeding structure and the dipole. The dipoles can be connected to the ground plane primarily through two pairs of rectangular patches, which are placed vertically in the EBG structure and attached to one side of the feeding line. On the other side of the balun, the inverted L-shaped feeding line is also placed vertically in the EBG surface and is used

Submitted On: October 19, 2020
Accepted On: November 29, 2020

https://doi.org/10.47037/2020.ACES.J.351208

to excite the antenna. The half ring shape of the two inverted L-shaped feeding lines is intended to reduce coupling between the ports, where the bottom ends of the feeding lines are connected to the SMA connectors in Fig. 2.

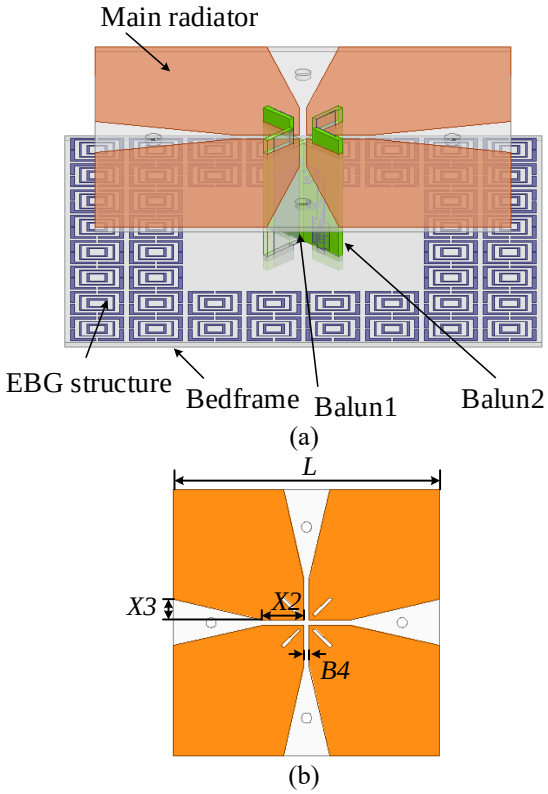

Fig. 1. (a) 3-D view of the proposed antenna, and (b) geometry of the patch.

In order to better understand the working principle of the feeding lines, the equivalent ac circuit diagram of the feeding structure is given in Fig. 3. In the feeding structure, the open branches, branch1 and branch2, can be equivalent to LC resonance circuit. Each open branch can be equivalent to LC resonant circuit, among which the resonance point of branch1 and branch2 are 3.8 GHz and 4.45 GHz, respectively. Series resonance circuits suppress harmonics when they resonate. Moreover, the slot coupling can be seen as inductance.

Figure 4 shows the geometric structure of the designed EBG array and a single EBG unit. The rectangular slots are made in a square patch, which form the EBG structure we designed. The CRR-EBG structure belongs to Uni-planar Compact EBG (UC-EBG). The CRR-EBG can be equivalent to a parallel LC model, the resonant frequency of which lends the high-impedance band-gap characteristics to the CRR-EBG structure, as shown in formulas (1) and (2):

$$w_0 = \frac{1}{\sqrt{LC}}, \tag{1}$$

$$z_s = \frac{j\omega L}{1-w^2 LC}. \tag{2}$$

A 26mm diameter cylinder is subtracted from the reflector to make it easier connected with SMA connector in actual measurement. The antenna is analyzed and optimized by HFSS 15, and the optimal values defined in Figs. 1 and 2 are listed as follows (unit: mm): *X2*=12, *X3*=6, *B4*=1.5, *L*=78, *M3*=14, *D4*=7, *W4*=4.6, *W5*=1.3, *D5*=2.8, *D7*=10, *W6*=2.4, *Rin*=1.7, *Rout*=4.1, *L5*=20, *BL*=6, *H1*=28, *W1*=2.25, *D1*=5, *D2*=9, *BW2*=5.8, *W7*=1.8735, *BW*=3, *GL*=164, *GH*=8, *T*=1, *N*=0.32, *We*=0.48, *M*=8.5, *A*=10, *L3*=89.4.

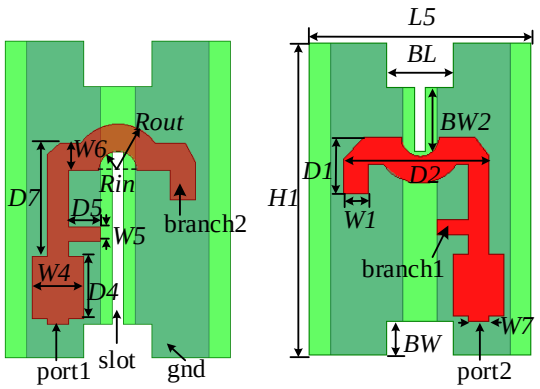

Fig. 2. Feeding structure for port1 and port2.

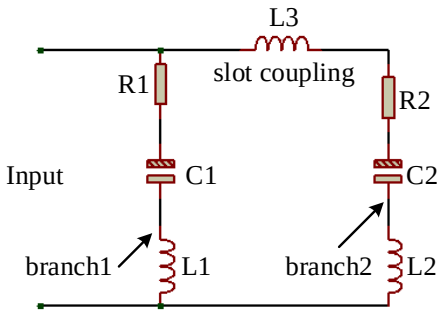

Fig. 3. Equivalent AC circuit diagram of the feeding structure.

Figure 5 shows a comparison of simulated S_{11} values for the dual-polarized dipole with and without an EBG structure for port1. It can be observed from Fig. 5 that the EBG structure has a great impact on impedance matching. When the EBG structure is not added, the impedance bandwidth is narrow with low frequency (3.02–3.15 GHz) and high frequency (4.1–4.74 GHz) for $S_{11} \leqslant -10$dB. By adding the EBG structure, a wide impedance bandwidth from 3.14 to 4.8 GHz is realized.

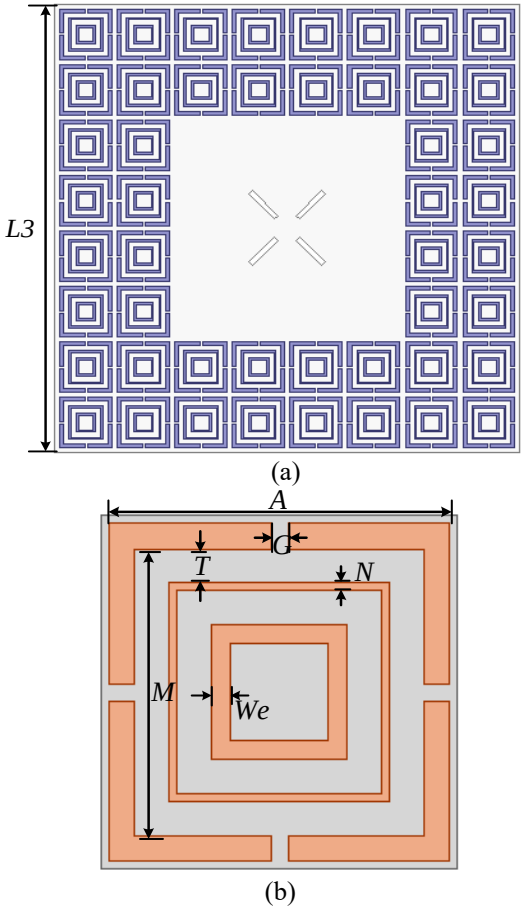

Fig. 4. (a) EBG array (b) geometry of the single EBG unit.

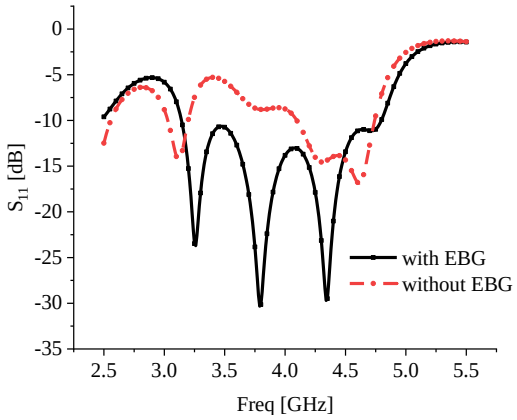

Fig. 5. Comparison of proposed antenna with and without EBG structure.

III. RESULTS AND DISCUSSION

S-parameters in this work were measured by a network analyzer. Gain and radiation patterns were measured in an OTA anechoic chamber. As shown in Fig. 6 (a), simulated and measured S-parameters of the antenna are given for port1 and port2. As can be seen from the S-parameter diagram, the simulated bandwidth is 37% (3.13-4.55GHz) and 34.1% (3.13-4.42GHz) for port1 and port2, respectively while the measured bandwidth is 28.3% (3.13-4.16GHz), the center frequency being 3.64 GHz. As can be seen from the simulated and measured results, the reflection coefficients are different at the two ports. The main reasons are as follows. First, the structure of the feeding lines at the two ports is not completely the same, especially for the ring part. Second, uneven welding resulted in a non-parallel state between the planes, having a strong impact on the reflection coefficients. The simulated and measured gains and isolation degree are presented in the Fig. 6 (b). The isolation performance in the operating band is better than 23 dB and the simulated gain is about 5 dBi. Furthermore, the bandwidth of the antenna with EBG is widened because of its leaky region. The experimental results are in good agreement with the simulation results.

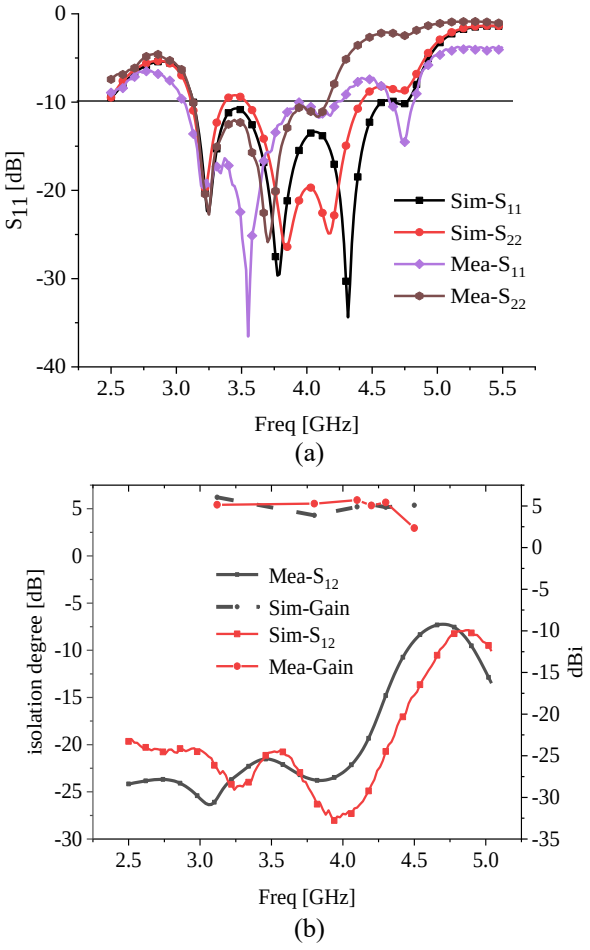

Fig. 6. Simulated and measured S-parameters of antenna.

Figure 7 shows the comparison of simulated and measured radiation patterns of the design at the frequencies of 3.12, 3.80 and 4.5 GHz, respectively. At 3.12 GHz, the radiation pattern consistency between simulation and measurement is relatively high. Among them, the radiation patterns are relatively stable at 3.8 GHz and 4.5 GHz. It can be seen from the direction diagram that the gain is about 4.8 dBi, and the directivity of the simulated and measured radiation patterns is consistent. Figure 8 presents the fabricated prototype of the antenna as well as the antenna test scenario. Compared with the antenna without EBG structure in [8], the proposed antenna broadens the frequency band, and improves the stability of the antenna radiation pattern.

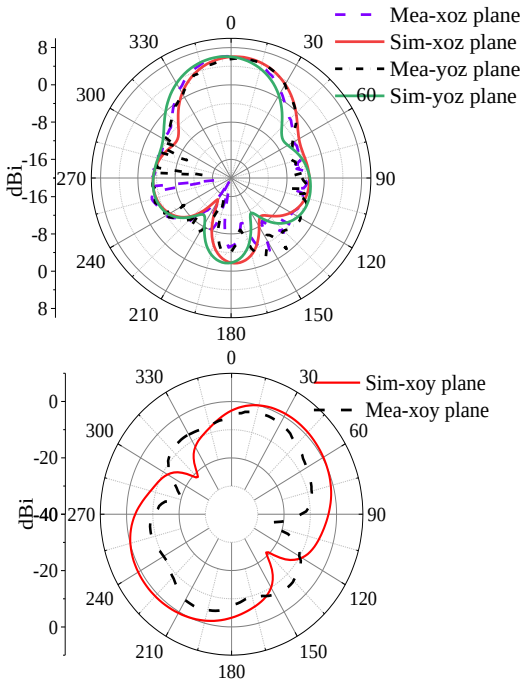

(a) 3.12GHz

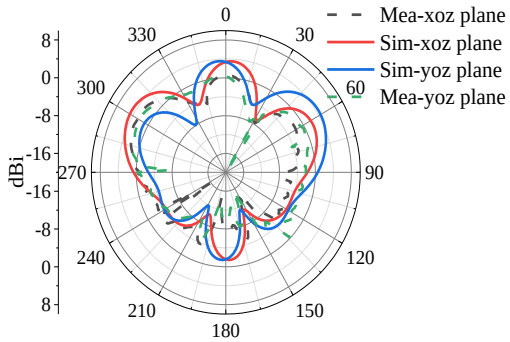

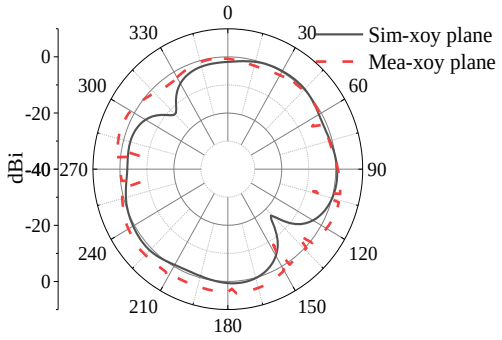

(b) 3.8GHz

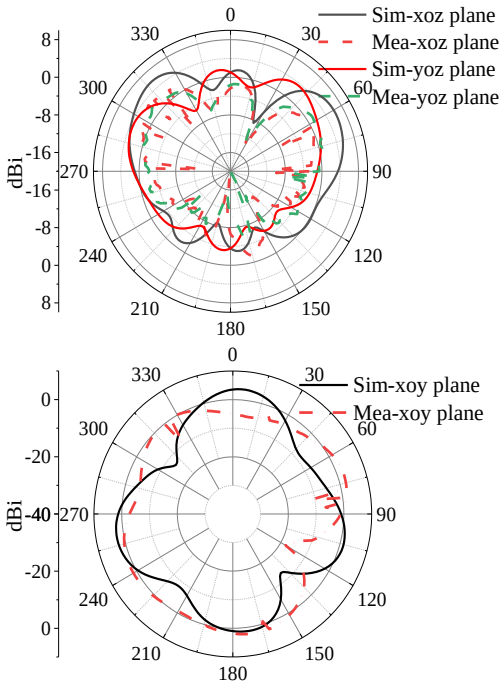

(c) 4.5GHz

Fig. 7. Simulated and measured radiation pattern of antenna: (a) 3.12 GHz, (b) 3.8 GHz, and (c) 4.5 GHz.

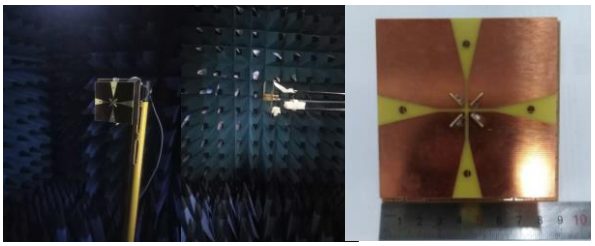

Fig. 8. Antenna in test and fabricated prototype of the antenna.

Table1: Comparison of the proposed antenna with references

Ref.	Bandwidth (GHz)	Gain (dBi)	Isolation	Type of EBG
[8]	3.12-3.68	5.84	＞23.5	/
[10]	3.16-3.48	/	＞30	TVS-EBG
[15]	3.31-4.33	/	＞20	CSRR-EBG
[19]	3.60-4.06	/	＞20	ELV-EBG
Pro.	3.13-4.42	5	＞23	CRR-EBG

λ_0 is the wavelength in free space at center operating frequency.

In Table 1, the performance of the proposed antenna is compared with previously published antennas. The antenna's bandwidth of our design operates 3.1 to 4.42 GHz, which is wider than that published references. The port-to-port isolation is slightly higher than [15] and [19]. But the gain is lower than that of Ref. [8]. To sum up, the performance of the antenna is better than other references in the table.

IV. CONCLUSION

A wideband dual-polarized base station antenna with EBG structure is presented herein, where the leaky wave region of EBG has been used to expand the frequency band and yield a stable radiation pattern of the antenna. The loop design of the feeding structures proves to be capable of reducing port coupling significantly. The antenna operates in the frequency band of 3.13-4.16 GHz. Simulated results prove that the design has the advantages of good bandwidth, stable radiation pattern and high isolation degree. Future work will be focused on further optimization of the radiation patterns and other antenna performance.

ACKNOWLEDGMENT

This work was supported by Natural Science Foundation of Fujian Province (Grant No. 2020J02042, 2019J01718 and 2018J05109).

REFERENCES

[1] C. Lei, L. L. Chen, J. Q. Zhang, and L. Dan, "A broadband dipole antenna with parasitic patch loading," *IEEE Antennas Wirel. Propag. Lett.*, vol. 17, pp. 1717-1721, Sept. 2018.

[2] G. Feng, L. Chen, X. Wang, X. Xue, and X. Shi, "Broadband circularly polarized crossed bowtie dipole antenna loaded with parasitic elements," *IEEE Antennas Wirel. Propag. Lett.*, pp. 114-117, Jan. 2018.

[3] J. Tao, Q. Feng, and L. Tao, "Dual-wideband magnetoelectric dipole antenna with director loaded," *IEEE Antennas Wirel. Propag. Lett.*, vol. 17, no. 10, pp. 1885-1889, Oct. 2018.

[4] X. Chao, J. Yin, L. Xiang, P. Feng, and Y. Jian, "An ultrawideband dipole with a director as a feed for reflector antennas," *IEEE Antennas Wirel. Propag. Lett.*, vol. 16, no. 99, pp. 1341-1344, Dec. 2017.

[5] C.-W. Hsiao and W.-S. Chen, "Broadband dual-polarized base station antenna for LTE/5G C-band applications," *The 2018 Cross Strait Quad-Regional Radio Science and Wireless Technology Conference (CSQRWC)*, Xuzhou, China, July 2018.

[6] Y. Li, W. Li, and W. Yu, "A multi-band/UWB MIMO/diversity antenna with an enhanced isolation using radial stub loaded resonator," *Appl. Comput. Electromagn. Soc. J.*, vol. 28, no. 1, pp. 8-20, Jan. 2013.

[7] K. L. Chung, X. Yan, and Y. Li, "A Jia-shaped artistic patch antenna for dual-band circular polarization," *AEU-International Journal of Electronics and Communications*, vol. 120, article ID 153207, June 2020.

[8] P. Chen and L. Wang, "A dual-polarized sakura-shaped base station antenna for the fifth generation (5G) communications," *Appl. Comput. Electromagn. Soc. J.*, vol. 35, no. 5, pp. 567-571, May 2020.

[9] D. Su, J. J. Qian, Y. Hua, and D. Fu, "A novel broadband polarization diversity antenna using a cross-pair of folded dipoles," *IEEE Antennas Wireless Propagation Letters*, vol. 4, pp. 433-435, Dec. 2005.

[10] P. P. Bhavarthe, S. S. Rathod, and K. T. V. Reddy, "A compact two via slot-type electromagnetic bandgap structure," *IEEE Microw. Wirel. Compon. Lett.*, vol. 27, no. 5, pp. 446-448, May 2017.

[11] L. Peng, C.-L. Ruan, and Z.-Q. Li, "A novel compact and polarization-dependent mushroom-type EBG using CSRR for dual/triple-band applications," *IEEE Microw. Wirel. Compon. Lett.*, vol. 20, no. 9, pp. 489-491, Sept. 2010.

[12] S. Y. Luo, Y. S. Li, Y. F. Xia, and L. Zhang, "A low mutual coupling antenna array with gain enhancement using metamaterial loading and neutralization line structure," *Appl. Comput. Electromagn. Soc. J.*, vol. 34, no. 3, pp. 411-418, 2019.

[13] M. J. Al-Hasan, T. A. Denidni, and A. R. Sebak, "Millimeter-wave EBG-based aperture-coupled dielectric resonator antenna," *IEEE Trans. Antennas Propag.*, vol. 61, no. 8, pp. 4354-4357, Aug. 2013.

[14] T. Jiang, T. Jiao, and Y. Li, "A low mutual coupling MIMO antenna using periodic multi-layered electromagnetic band gap structures," *Appl. Comput. Electromagn. Soc. J.*, vol. 33, no. 3, pp. 305-311, Mar. 2018.

[15] L. Peng, C.-L. Ruan, and Z.-Q. Qiang, "A novel compact and polarization-dependent mushroom-type EBG using CSRR for dual/triple-band applications," *IEEE Microw. Wirel. Compon. Lett.,* vol. 20, no. 9, pp. 489-491, Sept. 2010.

[16] C. Ding, H. Sun, Y. Guo, P. Qin, and Y. Yang, "Beamwidth control of base station antennas employing reflectors and directors" *2015 International Symposium on Antennas and Propagation (ISAP)*, Hobart, TAS, Australia, Nov. 2015.

[17] H. Huang, Y. Liu, and S. Gong, "A broadband dual-polarized base station antenna with anti-interference capability," *IEEE Antennas Wirel. Propag. Lett.*, vol. 16, pp. 613-616, July 2016.

[18] Z. Nie, H. Zhai, L. Liu, J. Li, D. Hu, and J. Shi, "A dual-polarized frequency-reconfigurable low-profile antenna with harmonic suppression for 5G application," *IEEE Antennas Wirel. Propag. Lett.*, vol. 18, no. 6, pp. 1228-1232, June 2019.

[19] E. Rajo-Iglesias, L. Inclan-Sanchez, J.-L. Vazquez-Roy, and E. Garcia-Muoz, "Size reduction of mushroom-type EBG surfaces by using edge-located vias," *IEEE Microw. Wirel. Compon. Lett.*, vol. 17, no. 9, pp. 670-672, Sept. 2007.

[20] Y. Li, W. Li, and Q. Ye, "A reconfigurable triple-notch-band antenna integrated with defected microstrip structure band-stop filter for ultra-wideband cognitive radio applications," *Int. J. Antennas Propag.*, vol. 2013, p. 13, article ID 472645, 2013.

[21] J. Jiang, Y. Xia, and Y. Li, "High isolated X-band MIMO array using novel wheel-like metamaterial decoupling structure," *Appl. Comput. Electromagn. Soc. J*, vol. 34, no. 12, pp. 1829-1836, Dec. 2019.

[22] K. L. Chung, X. Yan, A. Cui, and Y. Li, "Circularly-polarized linear antenna array of non-identical radiating patch elements for WiFi/WLAN applications," *AEU-International Journal of Electronics and Communications*, article ID 153526, Nov. 2020.

[23] M. Kim, "A compact EBG structure with wideband power/ground noise suppression using meander-perforated plane," *IEEE Trans. Electromagn. Compat*., vol. 57, no. 3, pp. 595-598, June 2015.